13th International Symposium on Turbulence and Shear Flow Phenomena (TSFP13)
Montreal, Canada, June 25-28, 2024

JET CONTROL USING DISTRIBUTED MINIJETS: REYNOLDS NUMBER EFFECT AND SCALING

Fan Dewei
Center for Turbulence Control,
Harbin Institute of Technology, Shenzhen
fandewei2014@hotmail.com

Du Jianjun
School of Mechanical Engineering and Automation,
Harbin Institute of Technology, Shenzhen
jjdu@hit.edu.cn

Wu Zhi
Center for Turbulence Control,
Harbin Institute of Technology, Shenzhen
wuzhiabcd@163.com

Zhou Yu
Center for Turbulence Control,
Harbin Institute of Technology, Shenzhen
yuzhou@hit.edu.cn

ABSTRACT

This work aims to investigate experimentally the effect of Reynolds number *Re* on and scaling of jet control using six independent unsteady radial minijets, with a view to enhancing jet mixing. A hybrid artificial intelligence (AI) control system that incorporates both genetic programming and genetic algorithm has been deployed to manipulate a jet whose *Re* varies in the range of 4,000-24,000 based on the jet exit velocity $\overline{U}_j$ and nozzle exit diameter *D*. The control parameters include the mass flow rate ratio $C_{m,i}$, the excitation frequency f_e and duty cycle α_i of each minijet (i = 1, 2, ..., 6), with an exit diameter of *d*. Jet mixing is quantified using K/K_0, where *K* is the decay rate of the jet centreline mean velocity, and the subscript '0' denotes the unforced jet. The learning process of AI control discovers four typical forcings, i.e. axisymmetric, helical and flapping, one by one in the order of increased performance, and finally converges to a forcing featured by both helical motion around a nonstationary switching axis and three-dimensional flapping, irrespective of *Re*. Empirical scaling analysis of experimental data, generated in the learning process, reveals that the relationship $K = g_1(C_{m,i}, \alpha_i, Re, d/D, K_0)$ may be reduced to $K/K_0 = g_2(\zeta)$, where $\zeta = (\xi/Re)^m$ and $\xi = \sum_{i=1}^{6}(C_{m,i}/\alpha_i)(d/D)^{n-1}$, n and m are power indices, g_1 and g_2 are the nonlinear function. The physical meaning of ξ is discussed, along with some interesting inferences from the scaling law.

INTRODUCTION

The turbulent jet is one of classical flows discussed in virtually every fluid mechanics textbook. Jet control can be passive and active. The former requires no power input, such as changing the geometric shape of nozzles, which is efficient and reliable. The latter, such as speaker- or plasma-based and fluidic actuation, needs additional power input but may achieve more flexible and drastic flow modifications than the former. Over the past few decades, many active techniques have been proposed to improve jet mixing. The one developed by Zhou *et al*. (2020) deploys an artificial intelligence (AI) control technique based on six unsteady minijet, exhibiting a great potential to increase jet mixing significantly further. Their jet manipulation led to the occurrence of a novel turbulent flow structure, never reported before, that outperformed significantly all the classical flow structures previously reported. Their work was demonstrated at a fixed Reynolds number (*Re* = 8,000). In another experimental study on jet mixing at different *Re*, Perumal *et al*. (2022) develop a hybrid AI system to optimize the actuation states and strength of an unsteady minijet and proposed a scaling law which governs the effect of *Re* on jet manipulation. Then, several questions naturally arise. Can we develop an AI control system that may optimize simultaneously both the actuation states and strength of six minijets under different *Re*? How does the maximum *K* change as *Re* increases? Can we obtain the four typical flow structure reported in Zhou *et al*. (2020) or more new turbulent structures in other *Re*? Could we find a control law that governs the relationship between *K* and the control parameters of six minijets at varying *Re*?

To address the questions raised above, a AI control system is developed to manipulate a turbulent jet based on six unsteady minijets, with a view to maximizing its mixing. The system can search simultaneously the near-optimal control laws and a time-independent parameter in spite of a variation in *Re*. The *Re* effect on control performance and the optimal control parameters are investigated over *Re* = 4,000 - 24,000. A scaling analysis is then performed based on the massive data produced from the AI system.

EXPERIMENTS DETAILS

Experimental rig consists of a turbulent round jet and six minijet actuators, as schematically shown in Figure 1. The *Re* of the main jet is 4,000-24,000, where $Re = \overline{U}_j D/\nu$, $\overline{U}_j$ is the jet centerline time-averaged velocity measured at the nozzle exit, ν is the kinematic viscosity of air and *D* = 20 mm is the diameter of the nozzle. The centre of the jet exit is set as the origin of a Cartesian coordinate system, where the *x*-axis is aligned with the streamwise direction (figure 1). Six unsteady minijets issued from orifices with a diameter of 1 mm are equidistantly placed around the main jet.

The mass flow rate of the minijet through the pinhole is driven by a mass flow controller (FLOWMETHOD FL-802) with a measurement range of 0-7 l/min, whose experimental uncertainty is no more than 1%. The duty cycle and frequency

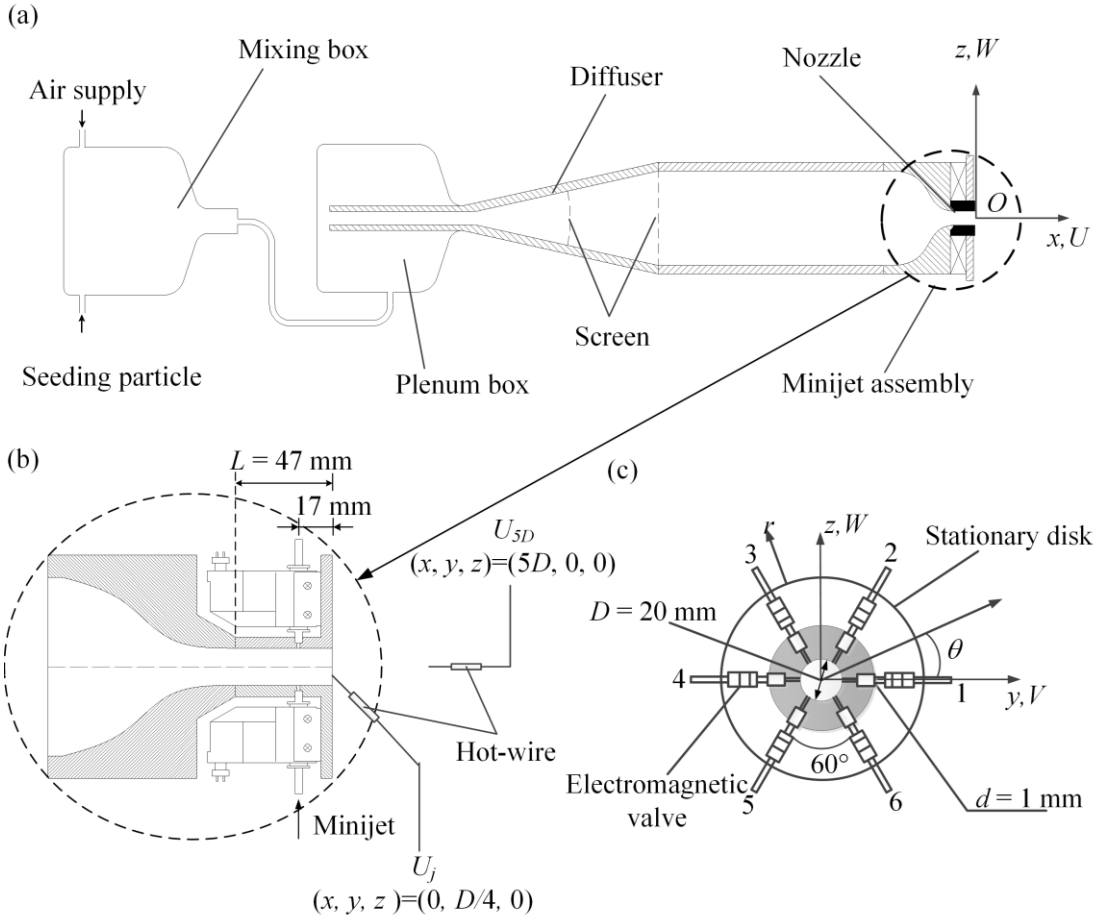

Figure 1. Schematic of experimental setup.

of the minijet injection are controlled using an electromagnetic valve that is operated on an ON/OFF mode with a maximum operating frequency of 500 Hz. The fluctuating flow velocity was monitored using two hot-wires placed at x/D = 0.05 and 5, respectively, operated on a constant temperature circuit at an overheat ratio of 1.8. The sampling frequency F_{RT} is 10 kHz. The experimental uncertainty in measured $\overline{U_j}$ is estimated to be within 2%.

The real-time control is implemented via a National Instrument PXI system. A LabVIEW Real-Time module is used for digitizing the analogue signal and providing control commends for the mass flow controller and electromagnetic valve. The same sampling rate is used for the velocity data acquisition and control command generation. As discussed in Fan & Zhou (2022), the available duty cycles are determined by F_{RT} and periodic excitation frequencies f_e.

HYBRID AI CONTROL SYSTEM

The main difference between conventional AI control system proposed by Zhou *et al*. (2020) and the hybrid AI control system is the modification of the control law composition. The AI can be performed in multi-frequency forcing mode or sensor-based feedback mode, depending on whether the control law consists of a series of harmonic signals or feedback signals. Following Zhou *et al*. (2020) and Perumal *et al*. (2022), the control law of the multi-frequency forcing mode can be represented as:

$$\boldsymbol{b}(t)=\boldsymbol{B}(\boldsymbol{h}(t),\boldsymbol{k}).$$

Here, $\boldsymbol{B}$ were functions for generating the actuation command based on the input harmonic functions $\boldsymbol{h}(t)$ and random constants $\boldsymbol{k}$. The argument $\boldsymbol{h}(t)$ is a set of harmonic functions, i.e.,

$$\boldsymbol{h}(t) = [h_1\ h_2\ \dots\ h_{11}]^T, \text{ where } h_i = \cos(2\pi f_i t).$$

Since the function $\boldsymbol{B}$ could be linear, quadratic or any other nonlinear function, a large range of frequencies can be generated in the control law signal. In general, the control law of multi-frequency forcing optimized by linear genetic programming (LGP) is a time-variant signal. For optimizing both driving signals of electro-magnetic valves and $C_{m,i}$, both the time-dependent signal and time-independent signal needs to be included in the control law. Usually, a genetic algorithm is suitable for optimizing $C_{m,i}$. In AI control system, the genetic programing operates on a population of computer programs (or functions) of varying sizes and shapes (Koza 1992). If we modify the population by replacing the time-dependent functions by time-independent functions, in principle, AI control system can optimize the time-independent signals as genetic algorithm.

Figure 2 shows the principle sketch of the hybrid AI control system. Following our previous work (Wu *et al*. 2018, Perumal & Zhou 2021, and Zhou *et al*. 2020), the cost function J is defined as $\overline{U}_{5D}/\overline{U}_j$ or 1-K, where $\overline{U}_{5D}$ is the time-averaged velocity measured at 5D downstream of the jet exit. The actuation command is denoted by $\boldsymbol{b}$, which contains two

independent laws, i.e., a time-dependent control law b_1 and a time-independent control law b_2.

$$\boldsymbol{b}(t) = [\boldsymbol{b}_1, \boldsymbol{b}_2]^T = [\boldsymbol{B}(h(t)), \boldsymbol{B}(h(t_0), k)]^T$$

On the one hand, the actuation command b_1 is transferred to binary values for driving electro-magnetic by using a Heaviside

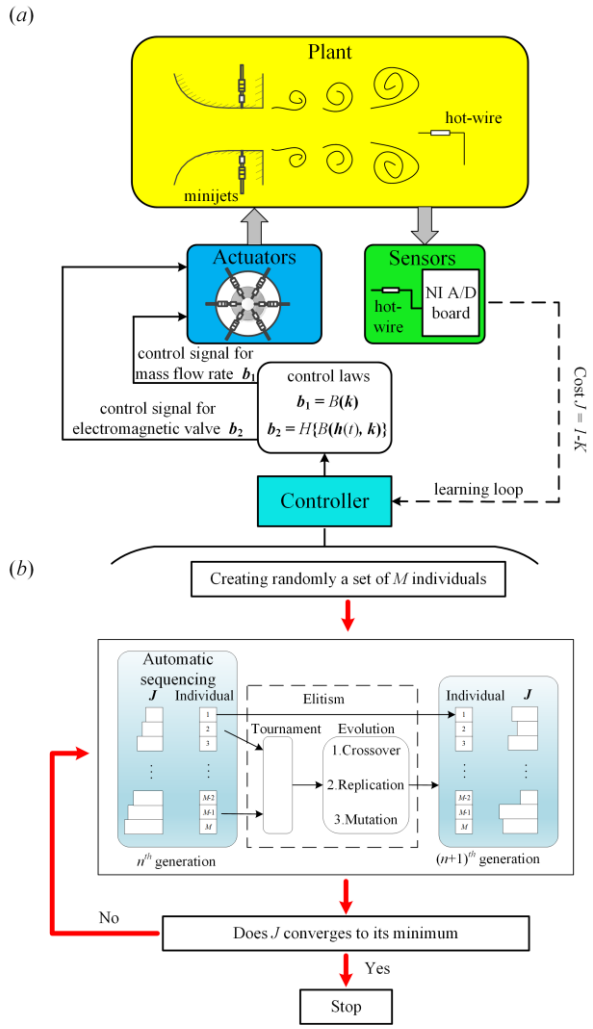

Figure 2. (*a*) Principle sketch of hybrid AI control system, which comprises the plant, sensors, actuators and a linear genetic programming controller (*b*) Schematic of linear genetic programming algorithm.

function H. On the other hand, the harmonic functions $h_i(t)$ in the b_2 is replaced by a constant value $h_i(t_0)$, where t and t_0 represents time and a constant factor, respectively. Thus, the time-independent control law $\boldsymbol{b}_2$ could be used for driving the $C_{m,i}$ of the pulsed minijet.

The control law optimization process using LGP is described briefly in figure 2*a*. Generally, hybrid AI acts as a regression solver to optimize a cost function associated with general nonlinear mappings, like the control law. The control system contains 4 steps: population creation (i.e., generate N_i=100 control laws), population evaluation (i.e., measure the performance of each control law), stop criterion check (i.e., check the best J) and population evolution (i.e., update generation based on the performance of last generation).

RESULTS AND DISCUSSION

Dependence of the maximum K, i.e. K_{max}, along with the corresponding control parameters under the optimal control law on Re were investigated (figure 3). K_{max} decreases from 0.78 to 0.7 when Re increases from 4000 to 8000, while K_{max} is found to be approximately a constant 0.7 for $Re \geq 8000$. However, the control parameters and performance K_{max}/K_0 exhibit a significant variation with Re. The optimum $C_{m,i}$ or $C_{m,i}^{opt}$ rises gradually from 1.09% to 6.7% from Re = 4000 to 24,000, suggesting a larger minijet momentum to maintain the penetration depth or the best control performance at a higher Re. Similar phenomena has also been found in Perumal *et al.* (2022). As expected, the values of K_{max}/K_0 are decreased from 33 to 11 when Re is increased from 4000 to 24,000.

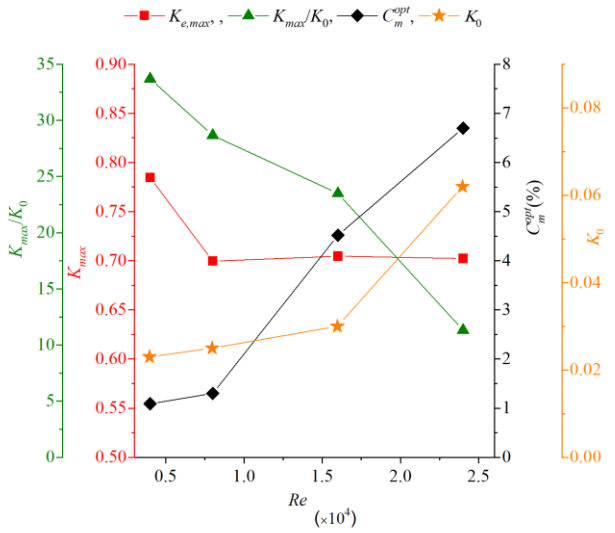

Figure 3. Optimal parameters achieved from the hybrid AI control system at different Re.

Figure 4(*a*) displays 3000 evaluated cost functions under AI control at Re = 8000. The unforced cost J_u is marked by a horizontal solid line. The squares at generation n = 1, ..., 30 mark the first and best individual of each generation with N_i = 100 individuals. The remaining costs of each generation are displayed by the increasing curve. Every curve has a unique color. The best individual of the first generation produces an axisymmetric control law. Subfigure (*a*1) shows the corresponding flow visualization. In the second generation, AI control discovers the helical forcing. The corresponding flow visualization (figure 4*a*2) shows a more regular pattern. In the fifth generation, AI control learns flapping forcing. Subfigure (*a*3) presents a strong flapping motion in *x*-*z* plane and a less pronounced mixing in the *x*-*y* plane which is symmetric with respect to the two synchronous actuator groups. In the eleventh generation, AI control discovers a combination of flapping and helical forcing, significantly outperforming the other forcings and resulting in a markedly reduction in decay rate. The corresponding flow visualization (figure 4*a*4) indicates the flapping mechanism. Intriguingly, these four control modes are also obtained for the other three Reynolds number Re = 4000, 16,000 and 24,000.

The control performance, evaluated by K, of the manipulating jet strongly depends on $C_{m,i}$, α_i and d/D when the excitation frequency ratio f_e/f_0 is fixed at 0.5; furthermore, the boundary-layer thickness at the jet exit diminishes with increasing Re, producing a significant influence on K_0, that is, K

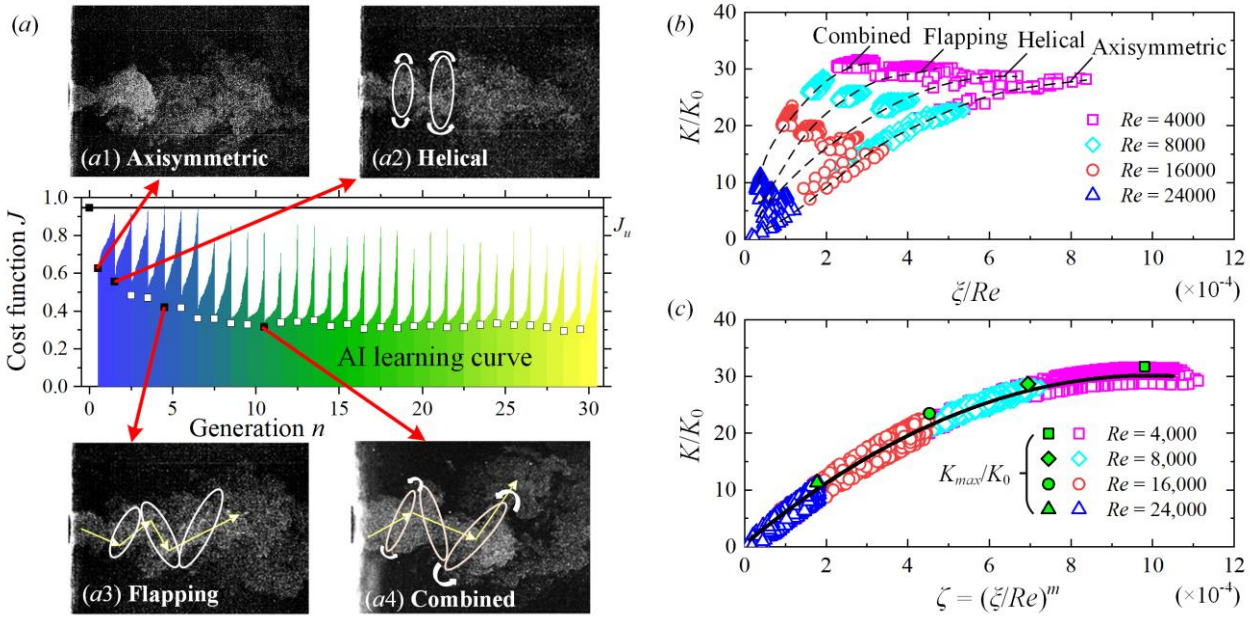

Figure 4. (*a*) The learning curve shows that the control law moves to the helical and flapping forcing from the axisymmetric forcing corresponding the streamwise flow visualization (*a*1-*a*4). Hollow square represents the best value for each generation. Dependence of K/K_0 on (*b*) ξ/Re and (*c*) $\zeta = (\xi/Re)^m$ for Re = 4000-24,000, α_i = 0.2 - 0.9, f_e/f_0 = 0.5, $C_{m,i}$ = 0-12%. The black curve is the least-squares fitting to experimental data.

is also a function of Re and K_0. After a careful analysis of the experimental data along with numerous trial-and-error attempts, it has been found that the relationship $K = g_1(C_{m,i}, \alpha_i, Re, d/D, K_0)$ can be reduced to $K/K_0 = g_3(\xi/Re)$, g_4 (ξ/Re), g_5 (ξ/Re) and g_6 (ξ/Re) given the same actuation phase shift φ, injection angle between the two adjacent jets θ, number of actived minijets N, where K/K_0 accounts for the control performance at a given Re, and $\xi = \sum_{i=1}^{6} (C_{m,i}/\alpha_i)(d/D)^{n-1}$ (the power index "n" depends on the Re and α) may be interpreted as the total momentum ratio per pulse of injection of six minijets. Following Perumal *et al.* (2022), the ξ/Re can be identified as a more general definition for the total effective momentum ratio of the six minijets to the main jet per pulse of injection in a varying Re. The scaling data are replotted in figure 4(*b*) showing the dependence of K/K_0 on ξ/Re. The data of K/K_0 displays a quite good collapse but branch into four, as evident by the dashed lines. Given $C_{m,i}$, α_i, f_e, Re and d/D, control laws can be divided into four modes, i.e. axisymmetric, helical, flapping and combined forcings. Then, the $K/K_0 = g_3(\xi/Re)$, g_4 (ξ/Re), g_5 (ξ/Re) and g_6 (ξ/Re) could be further reduced to $K/K_0 = g_2(\zeta)$, where $\zeta = (\xi/Re)^m$ and the power index "m" is associated with the control modes, i.e. m = 0.85 (combined), 0.9 (flapping), 0.95 (helical) and 1.01 (axisymmetric), respectively. Here, the ζ is physically the effective momentum ratio per pulse of the minijet injections to the inertia momentum of main jet, valid even in the context of varying Re. As shown in figure 4(*c*), almost K/K_0 collapses reasonably well once ζ is used as the abscissa, least-square-fitted by $K/K_0 = -3.0103172\times10^7\ \zeta^2 + 5.9839\times10^5\ \zeta + 0.45$. Note that given $C_{m,i}$, f_e, d/D, α_i and control mode (m), ζ may be calculated and hence K can be predicted from the equations over a range of Re (= 4000 – 24,000). This may have important applications in engineering.

Few interesting finds could be derived from the scaling law. On one hand, given the same ξ/Re, the control performance K/K_0 decreases as the control models factor m rises. It indicates that when the input power is fixed, the control performance only depends on the control modes. The jet mixing performance gradually improves as the control modes evolves from axisymmetric forcing (m = 1.01), helical forcing (m = 0.95), flapping forcing (m = 0.90), to the final combined forcing (m = 0.85). Thus, the combined forcing (the smallest m=0.85) could give the maximum K/K_0. On the other hand, if we fixed the control performance K/K_0, we can easily get the required ζ/Re. Given the $(d/D)^{n-1}$ and Re, the $\sum_{i=1}^{6} (C_{m,i}/\alpha_i)$, which indicates the input energy, is positively correlated with the factor m. In other words, smaller m needs lower power consumption to reach the same control performance.

CONCLUSIONS

A hybrid AI system has been applied to manipulate a jet using six pulsed radial minijets over a range of $Re \in$[4000, 24,000]. The AI system produces more than 4000 control laws for four Re's examined and subsequently a huge amount of data involving K and independent control parameters, i.e. $C_{m,i}$, α_i, Re, d/D and K_0. Major conclusions are drawn below:

The AI system exhibits good robustness as Re varies from 4000 to 24,000, finding K_{max} and the optimal control parameters. For example, AI system successfully finds the optimal control law at Re = 8000, which consists of seven sub-control laws that govern six time-dependent pulse signals (α_1 = 0.44, α_2 = 0.5, α_3 = 0.27, α_4 = 0.59, α_5 = 0.46, α_6 = 0.46, f_e/f_0 = 0.5) and a time-independent mass flow rate signal ($C_{m,i}$ = 1.2%), respectively, and hence K_{max} (= 0.7). K_{max} decreases from 0.78 in the laminar/transitional regime (Re = 4000) to 0.7 in the turbulent regime (Re = 8000) and remains unchanged for further increase in Re. The present K_{max} is appreciably larger than that (0.52) obtained by Perumal *et al*. (2022) using a single unsteady minijet,

implying more effective enhancement of jet mixing using multiple minijets than a single minijet.

AI control has identified in its learning process four typical forcings, i.e. axisymmetric, helical, flapping forcings, and combined forcing featured by both helical motion around a nonstationary switching axis and three-dimensional flapping, one by one in the order of increased performances, irrespective of *Re*.

Careful analysis of experimental data, produced from the learning process of AI control, leads to the finding of a scaling law, that is, $K = g_1 (C_{m,i}, \alpha_i, Re, d/D, K_0)$ may be reduced to $K/K_0 = g_2 (\zeta)$, where $\zeta = (\xi/Re)^m$ and $\xi = \sum_{i=1}^{6} (C_{m,i}/\alpha_i)(d/D)^{n-1}$. The power index m is 1.01, 0.95, 0.9 and 0.85 for the axisymmetric, helical, flapping and combined forcings, respectively. The ζ is physically the momentum per pulse of the minijet injections to the inertia momentum of main jet, which may be also interpreted as the minijet penetration depth. Interesting inferences can be made from this scaling law. The power index m in the scaling law is physically related to the control modes of the six pulsed minijets. Given the same total effective momentum ratio, per pulse of injection ξ/Re, of the six minijets to the main jet, a smaller m could give a larger K/K_0. That is, under the same input power, the jet mixing performance gradually improves as the control modes evolves from axisymmetric forcing (m = 1.01), helical forcing (m=0.95), flapping forcing (m=0.90), to the combined forcing (m=0.85). Furthermore, given the same control performance K/K_0, a smaller m corresponds to a lower ξ/Re, implying a gradually improved control efficiency as the control mode transforms from the axisymmetric, helical, flapping, to combined forcing.

ACKNOWLEDGEMENTS

Authors wish to acknowledge support given to them from NSFC through grants 91952204, 12202123 and 12202124, from the Research Grants Council of the Shenzhen Government through grants JCYJ20210324132816040, GXWD20220811152110003 and from CGN-HIT Advanced Nuclear and New Energy Research Institute through Grant No. CGN-HIT202221.

REFERENCES

Fan, D., and Zhou, Y., 2022 “Scaling and classification of a minijet-manipulated turbulent jet”, *Physical Review Fluids*, 7, 074606.

Koza, J. R. 1992. Genetic Programming: On the Programming of Computers by Means of Natural Selection. Boston: The MIT Press.

Perumal, A. K. and Zhou, Y. 2021 Axisymmetric jet manipulation using multiple unsteady minijets. *Physics of Fluids*, 33 (6), 065124.

Perumal, A. K., Wu, Z., Fan, D., and Zhou, Y., 2022 “A hybrid artificial intelligence control of a turbulent jet: Reynolds number effect and scaling”, *Journal of Fluid Mechanics*, 942, A47.

Wu, Z., Wong, C. W. & Zhou, Y. 2018 Dual-input/single-output extremum-seeking system for jet control. AIAA J. 56 (4), 1463—1471.

Zhou, Y., Fan, D., Zhang, B., Li, R., and Noack, B., 2020 “Artificial intelligence control of a turbulent jet”, *Journal of Fluid Mechanics*, 897, A27.